Eur. Phys. J. D **8**, 49–58 (2000)

THE EUROPEAN PHYSICAL JOURNAL D

EDP Sciences

Inelastic cross-sections and natural lifetimes for the $6^2D_{3/2,5/2}$ and $8^2S_{1/2}$ states of Rb

A. Ekers[1,a], M. Głódź[2,b], J. Szonert[2], B. Bieniak[2], K. Fronc[2], and T. Radelitski[2]

[1] Institute of Atomic Physics and Spectroscopy, University of Latvia, Raina bulv. 19, 1586 Riga, Latvia
[2] Institute of Physics, Polish Academy of Sciences, Al. Lotników 32/46, 02-668 Warsaw, Poland

Received 1st December 1998 and Received in final form 17 May 1999

Abstract. The results of an experimental study of population dynamics following excitation of $6^2D_{5/2,3/2}$ and $8^2S_{1/2}$ states of rubidium are reported. Excitation transfer and quenching cross-sections in collisions with ground state rubidium atoms, and natural lifetimes have been measured. The experiment was performed in a vapour cell, using pulsed two-photon excitation and photon counting detection. The analysis of time dependent signals was based on a rate equation model in which transitions induced by thermal radiation have been accounted for. The measurements yielded following results: (1) 6^2D state J-mixing cross-section: $\sigma^{\mathrm{Rb-Rb}}_{6D_{5/2}\to 6D_{3/2}} = 9.2(2.1)\times 10^{-14}$ cm^2; (2) cross-sections for $8^2S \to 6^2D$ excitation transfer process: $\sigma^{\mathrm{Rb-Rb}}_{8S\to 6D} = 3.4(1.2)\times 10^{-14}$ cm^2; (3) quenching cross-sections: $\sigma^{\mathrm{Rb-Rb}}_{q,\,8S} = 12.8(3.4)\times 10^{-14}$ cm^2, $\sigma^{\mathrm{Rb-Rb}}_{q,\,6D_{3/2}} = 22.8(2.9)\times 10^{-14}$ cm^2, $\sigma^{\mathrm{Rb-Rb}}_{q,\,6D_{5/2}} = 14.1(5.7)\times 10^{-14}$ cm^2; (4) radiative lifetimes: $\tau_{8S} = 161(3)$ ns, $\tau_{6D_{3/2}} = 256(4)$ ns, $\tau_{6D_{5/2}} = 249(5)$ ns.

PACS. 34.50.Fa Electronic excitation and ionization of atoms (including beam-foil excitation and ionization) – 32.70.Cs Oscillator strengths, lifetimes, transition moments – 32.50.+d Fluorescence, phosphorescence (including quenching)

1 Introduction

The purpose of the present work has been to study the $8^2S_{1/2}$ and 6^2D_J states of Rb atoms with respect to the population/depopulation processes such as radiative decay and collisions which result in quenching and in excitation transfer between the states concerned.

Total collisional quenching cross-sections for the rubidium ^{2}S and ^{2}D states as well as J-mixing ($nlJ \to nlJ'$ transition) cross-sections for ^{2}D states have recently been discussed in a review [1], where results of theoretical approaches to describe various collisional processes are confronted with experimental data. Existing theoretical treatments based on the quasifree electron model explain the n-dependence of quenching cross-sections for high n values. However, most of the measurements have been performed for states with relatively low n-values, for which such model does not hold. In the absence of theoretical data many authors compare experimental J-mixing and quenching cross-sections with geometrical ones.

Collisional excitation transfer (ET) processes other than the quasielastic fine structure mixing have also been studied extensively during the last 30 years. Much effort has been devoted to understanding the so called energy pooling (EP) in alkalis, in which the excitation energy of two colliding resonance atoms is transferred to higher excited states:

$$\mathrm{X}^*(^2\mathrm{P}) + \mathrm{X}^*(^2\mathrm{P}) \to \mathrm{X}^{**}(n^2l) + \mathrm{X}(^2\mathrm{S}), \qquad (1)$$

and to ET in heteronuclear collisions, in which the excitation is transferred from one type of atom to another. The most recent studies in this field concern m_J and velocity selective EP cross-sections in sodium [2], J selective measurements of EP in caesium combined with thorough rate equation analysis with respect to various factors (*e.g.*, radiation trapping, optical pumping etc.), which may influence the experimentally measured values of the cross-sections [3,4], and ET involving heteronuclear collision partners [5,6]. The common feature of the above mentioned processes is that the colliding particles in entrance and exit channels are connected with their ground states or with each other by electric dipole transitions, and the ET is determined mainly by the dipole-dipole interaction [7–10], although it has been noted [2], that higher terms of multipole expansion may also be of importance.

[a] *Present address*: Universität Kaiserslautern, Fachbereich Physik, Postfach 3049, 67653 Kaiserslautern, Germany.
e-mail: ekers@physik.uni-kl.de
[b] e-mail: glodz@ifpan.edu.pl

The situation becomes different when one considers ET between the atomic ^{2}S and ^{2}D states (hereafter referred to as S-D *transfer*), in processes of the type

$$X^*(^2S) + X(^2S) \leftrightarrow X^*(^2D) + X(^2S), \quad (2)$$

where atoms in neither channel possess dipole coupling. Intuitively one would expect that in this case the ET will be weak as determined by an interaction other than the dipole-dipole.

To our knowledge only a few experiments have been conducted on S-D transfer. A very high cross-section ($\sigma_{8S\to 6D} = 6.7 \times 10^{-13}$ cm^2) had been reported in [11] for the S-D transfer process

$$Rb(8^2S) + Rb(5^2S) \rightarrow Rb(6^2D) + Rb(5^2S) + \Delta E = +358\,\text{cm}^{-1}. \quad (3)$$

For Cs Rydberg states cross-sections were measured for ET from 9^2D, 10^2D to the 10^2S, 11^2S, and 12^2S states, and they are all of an order of 10^{-15} cm^2 [12]. Yet another study considers ET between the 7^2S and 5^2D states of rubidium [13], and the measured experimental cross-section $\sigma^{\text{exp}}_{7S\to 5D} = 8 \times 10^{-15}$ cm^2 was in reasonable agreement with the theoretical value $\sigma^{\text{th}}_{7S\to 5D} = 5.0 \times 10^{-15}$ cm^2 [14]. It should be noted, however, that in this case the rather high value of the S-D transfer cross-section was caused by the dipole-dipole interaction due to near lying $5^2P + 5^2P$ configuration, which introduced strong dipole coupling between the initial $7^2S + 5^2S$ and final $5^2D + 5^2S$ configurations of colliding atoms [14].

In sodium ET from 4^2D to 5^2S state was observed, and the corresponding cross-section was determined to be of the order of 10^{-15} cm^2 [15]. In that case one may also expect a strong influence of the $3^2P + 3^2P$ configuration, which lies between the $4^2D + 3^2S$ and $5^2S + 3^2S$ configurations.

For process (3), the influence of the $5^2P + 5^2P$ configuration can be neglected, since it is located more than 3000 cm^{-1} below the initial and final configurations. The surprisingly high $\sigma_{8S\to 6D}$, reported in [11], exceeds by a factor of four the value of the geometrical cross-section for 8^2S. Also the fact that in another study [16] the very same cross-section was reported to be 6.1×10^{-14} cm^2, which is an order of magnitude smaller than that obtained in [11], suggested that process (3) has to be reconsidered.

The natural lifetimes of excited states of atoms were extensively measured over several decades with continuously increasing precision due to technical development, as well as increasing awareness of side-effects influencing the measured values. Procedures have been developed to account for distorting phenomena such as magnetic field and/or polarisation effects [17,18], thermal escape [19], and the presence of blackbody radiation (BBR) [20].

A compilation of a vast number of experimental lifetimes for alkali atoms is contained in the paper by Theodosiou [21], who presents results of calculations for $n^2S_{1/2}$, n^2P_J, n^2D_J and n^2F_J alkali states with $n \leq 21$, and compares these lifetimes to the values measured by various authors and those calculated elsewhere. Theodosiou [21] and similarly Hansen [22] used a three term model potential. The first term, which is of different form in the two papers, represented the single-electron central field due to the nucleus and the core electrons, the second term accounted for core polarisation and the third for spin-orbit interaction. He *et al.* [23] used another simple model potential experienced by the valence electron. The agreement between theoretical and experimental lifetimes varies from state to state, which on the side of the experiment may be a consequence of neglecting one or another of above mentioned side effects affecting the measured values.

2 Experimental set-up and procedure

The experimental set-up is shown in Figure 1. The cylindrical Pyrex-glass cell, 90 mm high and 38 mm in diameter, containing a droplet of metallic rubidium was placed in a thermostabilised (to better than $\pm 0.2\,^\circ$C) two-chamber oven, and the temperature of its upper part T_u was varied between 75 and 125 °C. The temperature of the lower part of the cell was kept 5 °C below the temperature of the main oven body. The resulting atomic number density N_{Rb} ranged from 5.5×10^{11} to 1.5×10^{13} cm^{-3}.

The rubidium number density, N_{Rb}, was calculated by treating Rb vapour in the upper part of the cell as an ideal gas at a temperature T_u and at a pressure p_0 determined by the temperature T_l of the lower (colder) part with a droplet of Rb [24]. The temperature of the cell was continuously controlled by six chromel-alumel thermocouples attached to its surface. Temperature-vapour pressure relation from [25] was used to determine p_0, from which the Rb number density was calculated as $N_{Rb}(\text{cm}^{-3}) = 9.656 \times 10^{18} p_0(\text{torr})/T_u(\text{K})$. The cell was surrounded with a two-fold shield to screen the Earth's and stray magnetic fields. Two photon excitation on either $5^2S_{1/2} \rightarrow 8^2S_{1/2}$, $5^2S_{1/2} \rightarrow 6^2D_{3/2}$ or $5^2S_{1/2} \rightarrow 6^2D_{5/2}$ transitions was achieved by using radiation of an excimer laser pumped dye laser (Lumonics EX-520, HD-500, pyridine-1 dye, pulses of *ca.* 7 ns duration, spectral width of *ca.* 3 GHz). The linearly polarised laser beam with typical pulse energies of $40 \div 400\,\mu$J was sent through the cell. The nearly collimated and diaphragmed beam had a diameter of *ca.* 1 mm inside the cell. The fluorescence was observed at right angles. A two lens optical system imaged the fluorescence region onto the horizontal slit of a monochromator (Carl Zeiss Jena SPM2, dispersion 4 nm/mm, slit width 1.5 mm). The time-resolved fluorescence was detected with a cooled photomultiplier (Hamamatsu R943-02), followed by a fast preamplifier and a multichannel scaler (EG&G PAR 914P, channel width 5 ns). In order to ensure that relaxation of the population and not that of the alignment is being observed, a polarisation plane rotator in the laser beam path setting the laser polarisation direction at 54.7° from vertical orientation, and a vertically oriented polariser in the fluorescence path were used to provide the magic angle configuration (see, *e.g.*, [17]). A proper choice of the excitation-detection

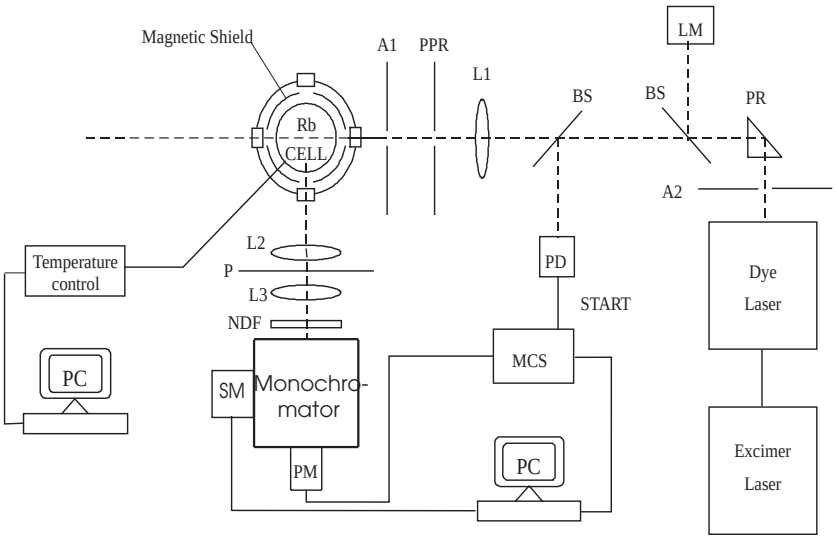

Fig. 1. Schematic diagram of the experimental apparatus: MCS – multichannel scaler; PM – photomultiplier; SM – stepping motor; PD – fast photodiode; LM – laser power meter; NDF – neutral density filter; L1–L3 – lenses; A1, A2 – apertures; PPR – polarisation plane rotator; P – polariser; BS – beam splitter; PR – prism.

geometry was evidenced by vanishing of hyperfine structure quantum beats in the time-resolved signals of the direct fluorescence from the $6^2\mathrm{D}_J$ states. The fluorescence was monitored on $8^2\mathrm{S}_{1/2} \to 5^2\mathrm{P}_{1/2}$, $6^2\mathrm{D}_{5/2} \to 5^2\mathrm{P}_{3/2}$, and $6^2\mathrm{D}_{3/2} \to 5^2\mathrm{P}_{1/2}$ transitions (607.1, 629.8, and 620.6 nm respectively). Background signals were also registered (see Sects. 4.1 and 4.2). Strong fluorescence signals were attenuated by spectrally calibrated neutral density filters to assure detector linearity. Relative spectral response of the detection system was measured over the wavelength range of interest using a calibrated tungsten ribbon lamp. All the data were corrected for these two factors.

Besides the time-resolved fluorescence, also emission spectra were registered with a photon counter (SR 430) with 2.5 μs wide time-gate delayed by 30 ns with respect to the laser pulse and tuning the monochromator in the vicinity of fluorescence lines of interest. The aim was to gather more information about spectral resolution and the origin of backgrounds. The spectra were taken with laser in resonance as well as detuned from the transitions.

3 Rate equations

3.1 J-mixing

Since the $6^2\mathrm{D}_{3/2}$ and $6^2\mathrm{D}_{5/2}$ levels are situated very close to each other (2.26 cm^{-1}), the J-mixing process can be treated in a framework of a quasi two-level system $|i\rangle$ and $|j\rangle$. The total decay rate Γ_i of state $|i\rangle$ can be written as a sum of radiative and collisional terms:

$$\Gamma_i = \Gamma_i^{\mathrm{rad}} + K_i^{\mathrm{out}} + R_{i\to j}, \tag{4}$$

where Γ_i^{rad} denotes the radiative decay rate, K_i^{out} is the rate of collisional ET from state $|i\rangle$ out of the two-level system, and $R_{i\to j}$ is the rate for ET from $|i\rangle$ to $|j\rangle$. The sum $K_i = K_i^{\mathrm{out}} + R_{i\to j}$ denotes the total collisional quenching rate of state $|i\rangle$.

The thermally averaged cross-sections $\sigma_{i\to j}$ considered in this paper are related to the relevant rates $R_{i\to j}$ as

$$R_{i\to j} = \sigma_{i\to j} N v, \tag{5}$$

where N is the number density of perturbing atoms, $v = \sqrt{8kT_{\mathrm{u}}/\pi\mu}$ is the mean relative velocity of the colliding partners, μ is their reduced mass, and k, the Boltzmann constant.

At the relatively low densities of our experiment, which result in ET rates much smaller than the radiative decay rates, one can neglect the effects due to multiple collisions. The duration of the laser pulse is much smaller than the relaxation times in the system. Under such conditions the time evolution of the populations in the laser excited level $|2\rangle$ and the collisionally excited level $|1\rangle$ after the exciting pulse is described by a simplified set of rate equations:

$$\frac{\mathrm{d}N_2}{\mathrm{d}t} = -\Gamma_2 N_2; \tag{6a}$$

$$\frac{\mathrm{d}N_1}{\mathrm{d}t} = R_{2\to 1} N_2 - \Gamma_1 N_1, \tag{6b}$$

with an initial condition $N_2(t=0) = N_{20}$, where $t = 0$ corresponds to incidence of the short laser pulse. To account for background signals, as explained in Section 4.1, we assume also some small initial population $N_1(t=0) = N_{10}$ for level $|1\rangle$. The detected fluorescence signals I_i are directly proportional to number density of atoms N_i in state $|i\rangle$:

$$I_i = \xi A_{iP} N_i. \tag{7}$$

Here, A_{iP} denote Einstein coefficients for the observed transitions to the resonance states, and proportionality coefficient ξ includes factors like collection efficiency and spectral response of the detection. We worked in the broad-slit limit, when the image of the fluorescing region

on the entrance slit of the monochromator is smaller than the slit width. Care was taken to ensure that the slit width used does not influence the sensitised to direct fluorescence signal ratio. All the registered signals were corrected for the spectral calibrations, while the geometry of the detection was kept unchanged during all the measurements. We assume therefore that the factor ξ is the same for all the detected wavelengths. The resulting from (6, 7) expressions for I_2 and I_1 are:

$$I_2 = \xi A_{2P} N_{20} \mathrm{e}^{-\Gamma_2 t}; \tag{8a}$$

$$I_1 = \xi A_{1P} \left(N_{10} \mathrm{e}^{-\Gamma_1 t} + N_{20} \frac{R_{2\to1}}{\Gamma_1 - \Gamma_2} (\mathrm{e}^{-\Gamma_2 t} - \mathrm{e}^{-\Gamma_1 t}) \right). \tag{8b}$$

In order to obtain the J-mixing rate and the corresponding cross-section (Eq. (5)), equations (8a, 8b) have to be fitted to the registered fluorescence signals.

The J-mixing cross-section can also be deduced by comparing the time integrals of sensitised ($\int_0^\infty I_1 \mathrm{d}t$) and direct ($\int_0^\infty I_2 \mathrm{d}t$) fluorescence signals, namely:

$$\eta = \frac{\int_0^\infty I_1 \mathrm{d}t}{\int_0^\infty I_2 \mathrm{d}t} = \frac{A_{1P}}{A_{2P}} \frac{1}{\Gamma_1} \left(\frac{N_{10}}{N_{20}} \Gamma_2 + R_{2\to1} \right). \tag{9}$$

The assumption $N_{10} = 0$ leads to the simple expression for the ET rate

$$R_{2\to1} = \eta \Gamma_1 \frac{A_{2P}}{A_{1P}} \cdot \tag{10}$$

3.2 $8^2S \leftrightarrow 6^2D$ transfer

In the course of analysis of the experimental data on $8^2S \leftrightarrow 6^2D$ ET we determined that the approximation of two levels interconnected by a single collisional ET rate is, unlike in the case of relatively strong J-mixing, not sufficient to correctly reproduce the shapes of the recorded time-resolved signals. We found it necessary to include in the analysis additional processes which compete with the direct ET between 8^2S and 6^2D. The two principal ones are induced by BBR[1]), with involvement of the intermediate states 7^2P and 8^2P, while the third process comprises ET between 8^2S and 5^2F. For example, on laser excitation to the 8^2S state, besides the direct ET, the population is transferred to the 6^2D state through (i) absorption of a BBR photon on the $8^2S \to 8^2P$ transition followed by emission to the 6^2D state; (ii) emission from 8^2S to 7^2P state followed by absorption of a BBR photon on the $7^2P \to 6^2D$ transition; (iii) ET from 8^2S to 5^2F followed by $5^2F \to 6^2D$ radiative decay (see Fig. 2).

In order to describe the time evolution of the population of relevant states, the equation system (6) is modified to

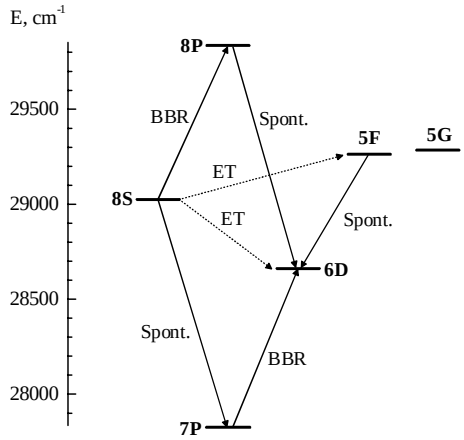

Fig. 2. Energy diagram of Rb and illustration of mechanisms of population transfer from the 8^2S to 6^2D state. "Spont." denotes prevailing spontaneous emission accompanied with few per cent of stimulated emission.

$$\frac{\mathrm{d}N_2}{\mathrm{d}t} = -\Gamma_2 N_2; \tag{11a}$$

$$\frac{\mathrm{d}N_1}{\mathrm{d}t} = -\Gamma_1 N_1 + R_{2\to1} N_2 + \sum_k T_{k\to1} N_k; \tag{11b}$$

$$\frac{\mathrm{d}N_k}{\mathrm{d}t} = -\Gamma_k N_k + T_{2\to k} N_2, \tag{11c}$$

where k denotes each of the three intermediate states 7^2P, 8^2P, 5^2F. For k corresponding to 7^2P and 8^2P, the rates T are expressed either as

$$T_{a\to b} = A_{ba} (g_a/g_b) \langle n_{ba} \rangle \tag{12a}$$

for absorption, or

$$T_{b\to a} = A_{ba} (1 + \langle n_{ba} \rangle) \tag{12b}$$

for emission (spontaneous and induced). When k denotes the 5^2F state, T is the collisional rate $T_{8S\to5F} \equiv R_{8S\to5F}$ (or $T_{5F\to8S} \equiv R_{5F\to8S}$) for the case when 8^2S (or 6^2D) is directly excited. g_a, g_b are the statistical weights of the states and $\langle n_{ba} \rangle = 1/(\exp(E_{ba}/kT) - 1)$ is the number of BBR photons per mode of energy E_{ba} equal to energy separation of the states.

By solving equations (11) with the initial conditions $N_2(t=0) = N_{20}$, $N_1(t=0) = N_k(t=0) = 0$ one obtains for N_1:

$$\begin{aligned} N_1 = N_{20} \Bigg(& \frac{R_{2\to1}}{\Gamma_2 - \Gamma_1} (\mathrm{e}^{-\Gamma_1 t} - \mathrm{e}^{-\Gamma_2 t}) \\ & + \sum_k T_{2\to k} T_{k\to1} \Bigg(\frac{1}{(\Gamma_2 - \Gamma_1)(\Gamma_k - \Gamma_1)} \mathrm{e}^{-\Gamma_1 t} \\ & - \frac{1}{(\Gamma_2 - \Gamma_k)(\Gamma_k - \Gamma_1)} \mathrm{e}^{-\Gamma_k t} \\ & + \frac{1}{(\Gamma_2 - \Gamma_k)(\Gamma_2 - \Gamma_1)} \mathrm{e}^{-\Gamma_2 t} \Bigg) \Bigg). \end{aligned} \tag{13}$$

[1] For Rydberg states the BBR driven transitions which strongly compete with the collisional ET are discussed in [20] and references therein.

The fluorescence signals I_i are related to the corresponding populations N_i by (7). Note, that I_2 is described, as before, by the single exponential function (8a).

3.3 Collisional quenching and radiative lifetimes

The fit of the single exponential (8a) to the direct fluorescence signal gives the total decay rate for this state at a certain temperature. This rate is related to the radiative decay rate and to the collisional quenching rate by (4). The procedure for extracting the natural lifetimes and quenching cross-sections at the conditions of the experiment is described in Section 4.3.

4 Results and analysis

4.1 J-mixing

To obtain the 6^2D state J-mixing cross-section, $\sigma^{\mathrm{Rb-Rb}}_{6\mathrm{D}_{5/2}\to 6\mathrm{D}_{3/2}}$, the $6^2\mathrm{D}_{5/2}$ state was excited, and both the direct fluorescence from $6^2\mathrm{D}_{5/2}$ and the sensitised fluorescence from $6^2\mathrm{D}_{3/2}$ were registered at various number densities of Rb atoms. For the sensitised fluorescence, which is much weaker than the direct fluorescence, the issue of background signals is very important. In order to identify their origin, the following steps were performed: (i) the noise signal was measured with the laser light blocked. This noise from sources like laboratory stray light or electronic pick-up from the laser discharge and trigger was negligible; (ii) the background was detected with the monochromator detuned from the line while laser remained on the resonance. The purpose was to determine the amount of the $6^2\mathrm{D}_{5/2} \to 5^2\mathrm{P}_{3/2}$ fluorescence passing at the wing of the transmission profile of the monochromator set at the $6^2\mathrm{D}_{3/2} \to 5^2\mathrm{P}_{1/2}$ transition wavelength. This background was still very small; (iii) the background was monitored with the laser 2-photon energy detuned down from the $5^2\mathrm{S}_{1/2} \to 6^2\mathrm{D}_{3/2}$ resonance by the amount equal to the 6^2D state fine structure splitting (2.26 cm^{-1}) and with monochromator set at the $6^2\mathrm{D}_{3/2} \to 5^2\mathrm{P}_{1/2}$ transition. In this case, we observed some direct 2-photon excitation of the $6^2\mathrm{D}_{3/2}$ state, which is most likely due to the excitation by broadband amplified spontaneous emission (ASE) present in the laser beam. The signal recorded in this way imitates the background to the measured sensitised fluorescence when the laser is in resonance with the $5^2\mathrm{S} \to 6^2\mathrm{D}_{5/2}$ 2-photon transition. The presence of the backgrounds (ii) and (iii) was evidenced also by analysing the emission spectra.

The parameters Γ_1, Γ_2, and ξN_{20} were obtained by fitting a single exponential (8a) to the direct fluorescence signals (see Sect. 4.3). Equation (8b) was then fitted to the sensitised fluorescence signals (see Fig. 3a), from where $R_{2\to 1} = R_{6\mathrm{D}_{5/2}\to 6\mathrm{D}_{3/2}}$ was obtained. Contribution of the direct excitation by ASE to the sensitised fluorescence was accounted for by allowing the second fitting parameter in equation (8b) $\xi N_{10} \neq 0$, which corresponds to direct excitation of the $6^2\mathrm{D}_{3/2}$ state during the laser pulse. In this way the admixture of the direct fluorescence from the $6^2\mathrm{D}_{5/2}$ state, whose lifetime is very close to that of the $6^2\mathrm{D}_{3/2}$, is also accounted for. The relevant Einstein coefficients were taken according to oscillator strengths given in [26].

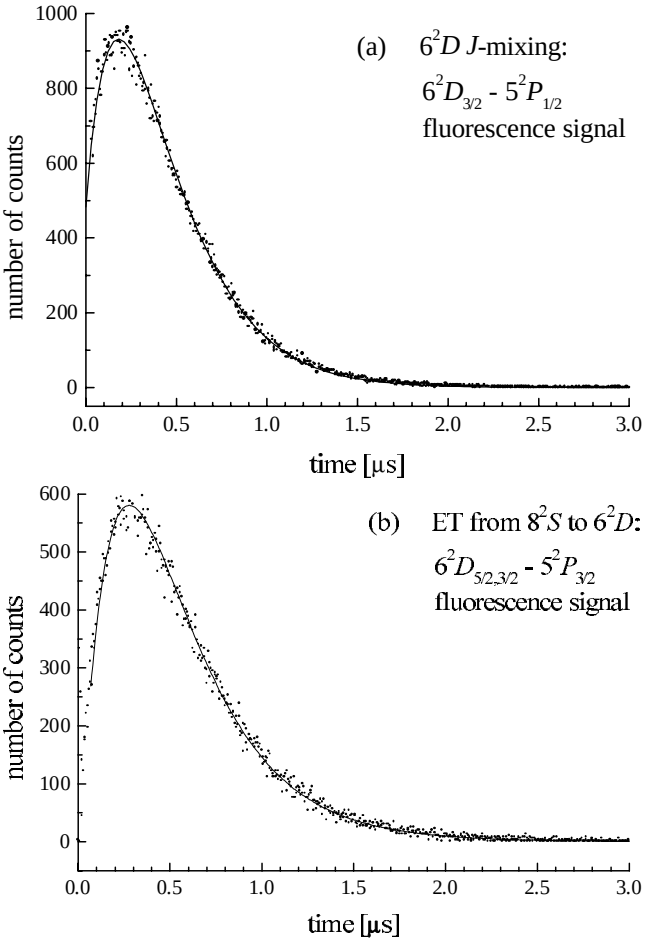

Fig. 3. Sensitised fluorescence signals: (a) from $6^2\mathrm{D}_{3/2}$ at laser excitation of the $6^2\mathrm{D}_{5/2}$ state; (b) from $6^2\mathrm{D}_{3/2,\,5/2}$ at laser excitation of $8^2\mathrm{S}_{1/2}$. Solid lines are least squares fits of equations (8b, 15) (with substitution of (13)), respectively.

We also tried another approach, to compare the time integrated signals according to equations (9, 10). To do this, the background recorded in separate measurements was subtracted from sensitised fluorescence signals. Although the $\mathrm{R}_{6\mathrm{D}_{5/2}\to 6\mathrm{D}_{3/2}}$ values obtained in this way did not differ significantly from those obtained by the former procedure, the scatter of points was larger. This suggests that the first method is more accurate, because it better compensates for an unknown amount of excitation by ASE.

By using the first approach, to fit the signal shapes, we also obtained strong evidence that there are no other mechanisms involved in the observed population transfer between the fine structure components except the direct collisional transfer. Otherwise it would not be possible to fit the shapes of the signals, since, according to (8b),

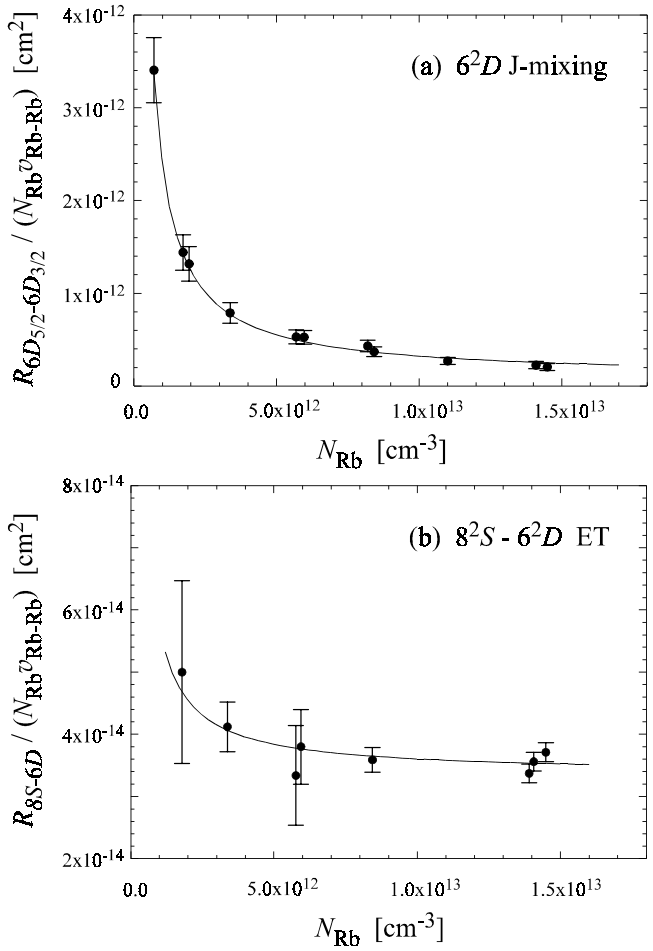

Fig. 4. The dependence on N_{Rb} of (a) $R_{6\mathrm{D}_{5/2}\to 6\mathrm{D}_{3/2}}/N_{\mathrm{Rb}}v_{\mathrm{Rb-Rb}}$ for $6^2\mathrm{D}_{5/2} \to 6^2\mathrm{D}_{3/2}$ J-mixing, (b) $R_{8\mathrm{S}\to 6\mathrm{D}}/N_{\mathrm{Rb}}v_{\mathrm{Rb-Rb}}$ for $8^2\mathrm{S} \to 6^2\mathrm{D}$ ET. • – experiment; solid line – least squares fit of equation (14) in case (a), and of an analogous one in case (b).

they are determined exclusively by the decay rates Γ_1 and Γ_2 of the states involved in the ET process.

Within the relatively narrow range of variation of $v_{\mathrm{Rb-Rb}}$ in the present experiment, the J-mixing cross-section due to Rb–Rb collisions was not expected to exhibit any noticeable dependence on temperature, and therefore on N_{Rb}. However, in Figure 4a a strong dependence of the cross-section values defined as $R_{6\mathrm{D}_{5/2}\to 6\mathrm{D}_{3/2}}/N_{\mathrm{Rb}}v_{\mathrm{Rb-Rb}}$ (Eq. (5)) on N_{Rb} is observed. This indicates that there is another process that contributes to the J-mixing and does not involve collisions with the ground state Rb atoms. The ratio of the respective time-integrated sensitised and direct fluorescence signals did not show any systematic dependence on the incident laser power, hence the eventual photoionisation of the $8^2\mathrm{S}$ and $6^2\mathrm{D}$ states cannot be suspected. Since the cell was baked out at 500 °C and evacuated for over two weeks until the residual pressure saturated at *ca.* 10^{-8} torr before a droplet of high purity rubidium was distilled into the cell and it was sealed off, the only foreign element could be atmospheric helium which can penetrate through the Pyrex-glass. The penetration rate increases rapidly as the temperature is increased (the rate increases by more than one order of magnitude as the temperature is raised from 25 °C by 100 °C [27]). Since the cell was kept at elevated temperatures during the previous experiments, the presence of certain amount of He in the cell is inevitable. We assumed therefore that the measured rate consists of two terms: $R_{6\mathrm{D}_{5/2}\to 6\mathrm{D}_{3/2}} = R^{\mathrm{Rb-Rb}}_{6\mathrm{D}_{5/2}\to 6\mathrm{D}_{3/2}} + R^{\mathrm{Rb-He}}_{6\mathrm{D}_{5/2}\to 6\mathrm{D}_{3/2}}$, where $R^{\mathrm{Rb-Rb}}_{6\mathrm{D}_{5/2}\to 6\mathrm{D}_{3/2}}$ is the rate for J-mixing in collisions with ground state Rb atoms, and $R^{\mathrm{Rb-He}}_{6\mathrm{D}_{5/2}\to 6\mathrm{D}_{3/2}}$ is the rate for J-mixing in collisions with He atoms (density N_{He}). Consequently,

$$\frac{R_{6\mathrm{D}_{5/2}\to 6\mathrm{D}_{3/2}}}{N_{\mathrm{Rb}}v_{\mathrm{Rb-Rb}}} = \sigma^{\mathrm{Rb-Rb}}_{6\mathrm{D}_{5/2}\to 6\mathrm{D}_{3/2}} + \sigma^{\mathrm{Rb-He}}_{6\mathrm{D}_{5/2}\to 6\mathrm{D}_{3/2}} N_{\mathrm{He}} \sqrt{\frac{\mu_{\mathrm{RbRb}}}{\mu_{\mathrm{RbHe}}}} \frac{1}{N_{\mathrm{Rb}}}, \quad (14)$$

where μ_{RbRb} and μ_{RbHe} are the reduced masses of colliding pairs of atoms (Rb–Rb) and (Rb–He). The resulting J-mixing cross-section, $\sigma^{\mathrm{Rb-Rb}}_{6\mathrm{D}_{5/2}\to 6\mathrm{D}_{3/2}} = 9.2(2.1)\times 10^{-14}$ cm^2, obtained by fitting equation (14) to the experimental points (solid line in Fig. 4a), is compared with the results of other studies in Table 1. The other fitting parameter was the factor $\sigma^{\mathrm{Rb-He}}_{6\mathrm{D}_{5/2}\to 6\mathrm{D}_{3/2}} N_{\mathrm{He}}$. Using the known cross-section for J-mixing induced by He, $\sigma^{\mathrm{Rb-He}}_{6\mathrm{D}_{5/2}\to 6\mathrm{D}_{3/2}} = 4.5(0.7) \times 10^{-14}$ cm^2 [28], we deduce the number density of He in our experiment to be $N_{\mathrm{He}} = 1.5(0.3)\times 10^{13}$ cm^{-3}, which is about one order of magnitude smaller than the helium atmospheric concentration. An independent estimate, based on available data on temperature-dependent transport of He through Pyrex [27], the registered periods of cell exposure to elevated temperatures during earlier experiments, and cell dimensions, gave $N_{\mathrm{He}} = 2(1) \times 10^{13}$ cm^{-3}, which is in a very good agreement with the former value.

The quoted error for the J-mixing cross-section results from the following contributions: (i) the statistical uncertainties from fitting the sensitised fluorescence signals with (8b), which vary from point to point in Figure 4a and are generally few per cent; (ii) the 4–7% uncertainty (from point to point) in the determination of the ASE-excitation contribution (factor ξN_{10}), which was deduced by comparing J-mixing rates obtained by the two above mentioned procedures (*i.e.*, fitting the time dependent fluorescence signals and calculating the ratios of time integrated fluorescence signals); (iii) the 6% inaccuracy of the relative spectral calibration; (iv) the 3% inaccuracy in the calibration of the neutral density filters used to attenuate direct and/or sensitised fluorescence signals; (v) uncertainty in the determination of the density of ground state Rb atoms. The latter consists of two contributions: (a) *ca.* 3% uncertainty due to ±0.5 °C inaccuracy in determination of the absolute temperature value, and (b) inaccuracy of the very Nesmeyanov's relation. Comparing the pressure calculated by using the empirical Nesmeyanov's formula [25] with Rb pressure reported

Table 1. Inelastic cross-sections for $Rb^* + Rb$ collisions, in units of 10^{-14} cm^2.

Initial state	Final state		Quenching cross section $\sigma_{q,i}^{Rb-Rb}$	Geometrical cross section σ_{geom}
	$6^2D_{3/2}$	$6^2D_{5/2}$		
$8^2S_{1/2}$	3.4(1.2)[‡,a] 67(30)[‡,d] 6.1(2.1)[‡,f]		12.8(3.4)[a] 8.1(2.0)[e]	15.7[g]
$6^2D_{3/2}$		13.8(3.2)[†,a] 10.4(2.1)[†,b] 17.3(3.5)[c]	22.8(2.9)[a] 25.3(5.3)[c]	11.7[g]
$6^2D_{5/2}$	9.2(2.1)[a] 6.9(1.4)[b] 11.6(2.3)[c]		14.1(5.7)[a] 15.6(3.3)[c]	

[a] This work.
[b] Parker et al., Ref. [36].
[c] Supronowicz et al., Ref. [28].
[d] Sharma et al., Ref. [11].
[e] Waligórski et al., Ref. [41].
[f] Barbier, Cherét, Ref. [16].
[g] Geometrical cross section is defined as, e. g., in Ref. [36].
[†] Recalculated using detailed balancing principle.
[‡] 6^2D fine structure not distinguished.

in some later papers [29–31] we estimate that for the temperature range of our experiment Nemeyanov's relation is accurate within 10%; (vi) the 18% statistical uncertainty of the cross-section value obtained from fitting the experimental points according to equation (14).

Possible contribution of BBR mediated transfer to the observed effective J-mixing was evaluated to be negligible. Associative ionisation in $Rb(6^2D) + Rb(5^2S)$ collisions, proceeding at a cross-section of $\sigma_{AI} = 3.4\times10^{-15}$ cm^2 [16], also gives negligible contribution to the observed population transfer between the 6^2D state J components. A detailed discussion of possible impact of ionisation processes on the population transfer is given in Section 4.2.1 regarding S-D transfer, and similar arguments apply also here.

4.2 $8^2S \leftrightarrow 6^2D$ transfer

Attempts were made to determine the cross-sections for ET between 8^2S and 6^2D in both directions. However, the analysis of time-resolved fluorescence allowed us to determine the cross-section only for the ET from 8^2S to 6^2D. Due to the negative energy defect and unfavourable ratio of the statistical weights, the opposite ET process is expected to be by a factor of 18 less efficient. The signals recorded by our apparatus in the $6^2D \rightarrow 8^2S$ case appeared to be masked by extra competing processes, which could not be unambiguously accounted for.

4.2.1 ET from 8^2S to 6^2D

With the $8^2S_{1/2}$ state excited by laser pulses, the sensitised fluorescence consisted of dominant fluorescence from the $6^2D_{5/2}$ state (the $6^2D_{5/2} \rightarrow 5^2P_{3/2}$ transition), overlapped with a fluorescence from the $6^2D_{3/2}$ state (the $6^2D_{3/2} \rightarrow 5^2P_{3/2}$ transition). The other component of the doublet from the $6^2D_{3/2}$ state (the $6^2D_{3/2} \rightarrow 5^2P_{1/2}$ transition) was overlapped with the strong $8^2S_{1/2} \rightarrow 5^2P_{3/2}$ line owing to low spectral resolution and therefore could not be detected. Assuming, in agreement with [11], that both 6^2D_J states are populated according to their statistical weights, g_J, a relation between the measured signal $I_{6D}^{meas} = I_{6D_{5/2}-5P_{3/2}} + I_{6D_{3/2}-5P_{3/2}}$ and the total population N_{6D} of the 6^2D doublet takes the form:

$$I_{6D}^{meas} = \xi N_{6D}\left(\frac{g_{5/2}}{g_{5/2}+g_{3/2}}A_{6D_{5/2}-5P_{3/2}} + \frac{g_{3/2}}{g_{5/2}+g_{3/2}}A_{6D_{5/2}-5P_{3/2}}\right), \quad (15)$$

where N_{6D} is given by equation (13). Along with the signal measurements background was also registered, with laser on (or off) resonance and monochromator detuned from (or tuned to) the transition. The background amounted 5–20% of the sensitised fluorescence signal (with relative uncertainty *ca.* 15%). The experimental $6^2D_{3/2,5/2} \rightarrow 5^2P_{3/2}$ fluorescence signals were corrected for the background, and the resultant decays were fitted with equation (15). $R_{8S\rightarrow6D}$ coming in from equation (13) was the only parameter of fit. Einstein coefficients $A_{6D_{5/2}-5P_{3/2}}$ and $A_{6D_{3/2}-5P_{3/2}}$ were taken according to [26]. Besides the direct ET, the two additional channels *via* the 7^2P and 8^2P states were included in (13). With the quenching cross-section of the 8^2S state (see Sect. 4.3) taken as an upper limit for $\sigma_{8S\rightarrow5F}$, we estimated that population transfer *via* the 5^2F state can be neglected because of the unfavourable $5^2F \rightarrow 6^2D$ branching ratio. Radiative rates $T_{8S\rightarrow k}$ and $T_{k\rightarrow6D}$ (12a, 12b) were obtained by using the Einstein coefficients based on [32]. Γ_{8S} and $\xi N_{20} \equiv \xi N_{8S}^0$ were obtained by fitting equation (8a) to the respective direct fluorescence signals (Sect. 4.3). Γ_{7P} and Γ_{8P} were taken according to [21].

Due to the presence of helium the values of $R_{8S\rightarrow6D}/N_{Rb}\nu_{Rb-Rb}$ exhibited a similar, though less pronounced, dependence on N_{Rb} (Fig. 4b) as in the case of J-mixing discussed above. Here also the ratio of the sensitised and direct fluorescence signals used in the analysis did not depend on the laser power. It is natural to fit the dependence in Figure 4b with a function of type (14) to account for the influence of collisions with He. This fit yielded the cross-section for Rb induced ET, $\sigma_{8S\rightarrow6D}^{Rb-Rb} = 3.4(1.2)\times10^{-14}$ cm^2 (see also Tab. 1). In the same time the cross-section for He induced ET was estimated as $\sigma_{8S\rightarrow6D}^{Rb-He} = 4.2(2.6)\times10^{-16}$ cm^2. This is to be compared with the value $1.3(0.5)\times10^{-16}$ cm^2, given in [11].

The total uncertainty of the SD-transfer cross-section, quoted in Table 1, results from similar sources of errors as in the case of J-mixing (see Sect. 4.1), with the difference that here the statistical errors and uncertainties due to the extraction of background are larger. Among the other

processes which may contribute to the population transfer, besides the above discussed excitation channel through the 5^2F state also a channel *via* molecular ions is possible. Such channel is open due to associative ionisation (AI) in Rb(8^2S) + Rb(5^2S) collisions followed by dissociative recombination of Rb_2^+ ions to the 6^2D state,

$$\mathrm{Rb}(8^2\mathrm{S}) + \mathrm{Rb}(5^2\mathrm{S}) \rightarrow \mathrm{Rb}_2^+ + e \rightarrow \mathrm{Rb}(6^2\mathrm{D}) + \mathrm{Rb}(5^2\mathrm{S}), \quad (16)$$

and the possible impact of this process can be evaluated as follows. Assuming that all the Rb_2^+ ions produced in the AI process ($\sigma_{\mathrm{AI}} = 4.6 \times 10^{-15}$ cm^2 [16]) dissociatively recombine to the 6^2D state, the value $\sigma_{8\mathrm{S}\rightarrow 6\mathrm{D}}^{\mathrm{Rb-Rb}}$ would be overestimated by 14%. In the reality recombination of Rb_2^+ ions leads to formation of both Rb_2 molecules and Rb atoms, spread over many excited levels, and the probability of recombination to just Rb(6^2D) is very little. Hence, the contribution of the process (16) can be safely neglected. A more likely way of population of 6^2D state is the radiative cascading of Rydberg atoms, produced in the ion recombination processes (including also the ions produced in photoionisation of the 8^2S state). Due to long lifetimes of highly excited states, such cascading processes would lead to presence of long decaying components with characteristic decay times of several tens of μs in the fluorescence signals. No such long decaying components were observed in the fluorescence signals, indicating, that this contribution can also be neglected.

It should be noted that the BBR mediated processes contribute significantly to the observed $8^2\mathrm{S} \rightarrow 6^2\mathrm{D}$ population transfer. Since the Rb number density is strongly dependent on temperature (Nesmeyanov's relation [25]), the relative contributions of BBR and collisionally mediated processes vary significantly with N_{Rb} (*i.e.*, with temperature). The ratio of both contributions (BBR mediated transfer to ET in Rb–Rb collisions) varies from a few at lowest N_{Rb} values to about one at highest N_{Rb} of the present experiment [33]. Therefore disregard of BBR in the analysis of the experimental results can lead to considerable errors.

4.2.2 ET from 6^2D to 8^2S

With both $6^2\mathrm{D}_J$ fine structure components consecutively excited, the direct $6^2\mathrm{D}_J \rightarrow 5^2\mathrm{P}$ and sensitised $8^2\mathrm{S} \rightarrow 5^2\mathrm{P}$ fluorescence was observed. However, in some cases we were unable to obtain a reliable fit of the function based on (13) to the 8^2S time-resolved fluorescence signals. In these cases, the fluorescence appeared to be considerably stronger than expected from the detailed balancing principle. According to (13), the shape of the time-resolved sensitised fluorescence (inclusive the BBR contribution) should be essentially the same for ET in directions opposite to each other. The difference is only in the amplitude scaling factor, which is unfavourable for the $6^2\mathrm{D} \rightarrow 8^2\mathrm{S}$ direction (*ca.* 18 times smaller). The process which might be responsible for the observed excess population of the 8^2S state is a superradiant (SR) transition from the laser excited 6^2D state to the 7^2P state, followed by the BBR induced transition to the 8^2S state. We could not observe with our detection system the IR superfluorescence emitted along the incident laser beam axis to unambiguously verify this possibility. We modelled this SR channel by introducing extra terms in (13), which allowed us to reproduce the shape of the 8^2S fluorescence signals [33]. Nevertheless we have omitted the results for $6^2\mathrm{D} \rightarrow 8^2\mathrm{S}$ transfer as less reliable. For the $8^2\mathrm{S} \rightarrow 6^2\mathrm{D}$ ET the extra terms revealed negligible effect on the $R_{8\mathrm{S}\rightarrow 6\mathrm{D}}$ values, showing that SR was not significant in that case.

4.3 Lifetimes and collisional quenching

To obtain $N_{\mathrm{Rb}} v_{\mathrm{Rb-Rb}}$-dependent total decay rates $\Gamma_{8\mathrm{S}}$, $\Gamma_{6\mathrm{D}_{3/2}}$ and $\Gamma_{6\mathrm{D}_{5/2}}$, each recorded direct fluorescence signal (total accumulated number of counts *ca.* 10^5 per curve) was repeatedly fitted by a single exponential equation (8a), while starting point of the decay curve was consecutively truncated at several points. The aim was to check if thus obtained resultant decay rates do not reveal any systematic changes. Some measurements were rejected upon this criterion. A mean value was adopted as a representative for a given decay, and standard deviation of the mean as its statistical uncertainty. The latter amounted 2–3%. Besides the predominant contribution of the spontaneous radiative decay, thus obtained rates contain also deexcitation rates due to (i) the presence of BBR, (ii) quenching induced by collisions with He atoms, and (iii) quenching induced by collisions with the ground state Rb atoms:

$$\Gamma_i = \frac{1}{\tau_i} + \Gamma_i^{\mathrm{bb}} + K_i^{\mathrm{Rb-He}} + K_i^{\mathrm{Rb-Rb}}.$$

Here, τ_i is the natural radiative lifetime; Γ_i^{bb}, the BBR induced transition rate [20]; $K_i^{\mathrm{Rb-He}} = \sigma_{q,i}^{\mathrm{Rb-He}} N_{\mathrm{He}} v_{\mathrm{Rb-He}}$ and $K_i^{\mathrm{Rb-Rb}} = \sigma_{q,i}^{\mathrm{Rb-Rb}} N_{\mathrm{Rb}} v_{\mathrm{Rb-Rb}}$ are the quenching rates in Rb–He and Rb–Rb collisions, respectively.

For each measurement, the corrected rate $\Gamma_i^{\mathrm{c}} = \Gamma_i - \Gamma_i^{\mathrm{bb}} - K_i^{\mathrm{Rb-He}}$ was calculated. The BBR corrections were performed as described in reference [34]. They amounted about 1% of the total decay rates. The contribution of He induced quenching was calculated for the $6^2\mathrm{D}_{3/2}$ and $6^2\mathrm{D}_{5/2}$ states using the respective cross-sections, $\sigma_{q,6\mathrm{D}_{3/2}}^{\mathrm{Rb-He}} = 6.6(1.0) \times 10^{-14}$ cm^2 and $\sigma_{q,6\mathrm{D}_{5/2}}^{\mathrm{Rb-He}} = 4.9(0.7) \times 10^{-14}$ cm^2, given in [28]. For the $8^2\mathrm{S}_{1/2}$ state we have not found in the literature any data on quenching by He. Therefore we adopted as a safe upper limit for this cross-section a value of 10^{-14} cm^2, which is based on available data for higher n values. The reliability of this assumption is supported by the results of the theoretical modelling presented in [35]. For the He number density we used the value $N_{\mathrm{He}} = 1.5(0.3) \times 10^{13}$ cm^3 determined in Section 4.1. Contributions to the observed rates due to collisions with He were on average 4%, 3% and 0.3% for the $6^2\mathrm{D}_{3/2}$, $6^2\mathrm{D}_{5/2}$ and $8^2\mathrm{S}_{1/2}$ states, respectively.

Table 2. Natural lifetimes for the $8^2S_{1/2}$, $6^2D_{3/2}$ and $6^2D_{5/2}$ states of Rb, in ns.

State	Experimental				Theoretical, 0 K		
	This work	MM[a,†]	LS[b,†]	WKR[c]	HLCZ[d]	Theodosiou[e]	Hansen[f]
$8^2S_{1/2}$	161(3)	154(7)	153(8)	166(4)	148	158.3	162.4
$6^2D_{3/2}$	256(4)		285(16)	234(7)[‡]	251[‡]	253.6	258.5
$6^2D_{5/2}$	249(5)	237(15)				243.7	244.1

[a] Marek, Münster, Ref. [39].
[b] Lundberg, Svanberg, Ref. [40].
[c] Waligórski et al., Ref. [41].
[d] He et al., Ref. [23].
[e] Theodosiou, Ref. [21].
[f] Hansen, Ref. [22].
[†] Not corrected for blackbody radiation
[‡] 6^2D fine structure not distinguished

Extrapolation of thus obtained corrected rates $\Gamma_i^{\rm c} = 1/\tau_i + \sigma_{q,i}^{\rm Rb-Rb} N_{\rm Rb} v_{\rm Rb-Rb}$ (Stern-Volmer plots) to the collisionless limit ($N_{\rm Rb} v_{\rm Rb-Rb} \to 0$) allowed us to obtain the natural lifetimes τ_i for all states of interest: $8^2S_{1/2}$, $6^2D_{3/2}$ and $6^2D_{5/2}$. From the slopes, the respective quenching cross-sections $\sigma_{q,i}^{\rm Rb-Rb}$ were determined. The results are listed in Tables 1 and 2 along with results available from other studies. The quoted errors were determined according to the following considerations. The error of a single point on the Stern-Volmer plot consists of three contributions: (i) the 2–3% statistical uncertainty of the decay curve analysis; (ii) uncertainty of helium-induced quenching rate (conservatively estimated to be 30%) which leads to inaccuracy of 1% for the $6^2D_{5/2}$ and $6^2D_{3/2}$ states, and negligible 0.1% for the 8^2S state; (iii) uncertainty of BBR correction, even if assumed large (20%), leads to small 0.2% error in the corrected rates. The resultant values obtained by fitting the Stern-Volmer plots are affected by statistical uncertainties of *max.* 0.5% for lifetimes and of *ca.* 10–40% for the respective quenching cross-sections. The indeterminacy of $N_{\rm Rb}$, which we estimated as 10% (see Sect. 4.1), has negligible effect on lifetime values, but influences the quenching cross-sections increasing their overall uncertainties.

5 Discussion

Inelastic cross-sections measured in this work are compared with available experimental results of other authors in Table 1. Our value for the 6^2D state J-mixing cross-section, $\sigma_{6D_{5/2}\to 6D_{3/2}}^{\rm Rb-Rb} = 9.2(2.1)\times 10^{-14}$ cm^2, is very close to average of those of the two other studies [28,36]. Strictly speaking, the cross-sections determined in the latter two studies do not overlap within their uncertainty limits. Our quenching cross-sections for both the $6^2D_{3/2}$ and $6^2D_{5/2}$ states are in agreement with the respective values measured in [28]. The 6^2D_J quenching is largely due to ET to the other J sublevel, though the contribution of ET out of the doublet is quite significant. A similar trend has been observed also for the other lowest ^{2}D states of rubidium (see, *e.g.*, the data compiled in [37]). The cross-section for ET from 8^2S to 6^2D amounts to only 1/4 of the total quenching of the 8^2S state. As far as other processes contributing to the quenching of 6^2D and 8^2S states are concerned, we can mention ET to the 5^2F and 5^2G states, the infrared fluorescence from which was beyond the sensitivity range of our detection (PMT), and associative ionisation in collisions with the ground state Rb atoms [16]. The contribution of the latter, however, does not exceed few per cent. $Rb^+ + Rb^-$ ion pair formation seems to be relatively inefficient as a quenching process [38].

The value for the $8^2S \to 6^2D$ ET cross-section, $\sigma_{8S\to 6D}^{\rm Rb-Rb} = 3.4(1.2)\times 10^{-14}$ cm^2, obtained by us is almost 20 times smaller than that measured in [11], and also smaller than the value (obtained as a side product of an ionisation experiment) reported in [16]. In neither of the studies [11,16] care was taken to account for the presence of thermal radiation. In present experiment the analysis of the shapes of time-resolved signals drew our attention to considerable contribution of extra channels due to the BBR-induced transitions. Account for the BBR mediated population transfer in the thermal conditions of experiments [11,16] would significantly lower the relevant cross-sections. In particular, the cross-section reported in [16] would become close to the present result, while the value of [11] would remain about ten times larger [33].

As mentioned in Section 1, the $8^2S \to 6^2D$ ET process is interesting, since here ET takes place between two configurations, which are not coupled by the dipole-dipole interaction. In the absence of calculated molecular terms correlating to these states, it is impossible to make definitive conclusions about the mechanism of this ET process. For the lower 7^2S and 5^2D states efficient mutual ET is possible thanks to the near lying $5^2P + 5^2P$ configuration which enables the dipole coupling between the $7^2S + 5^2S$ and $5^2D + 5^2S$ configurations [14]. For the 8^2S and 6^2D states, which are energetically distant from $5^2P + 5^2P$, ET was not expected to be particularly efficient. However, our measured cross-section for this process actually exceeds that for the ET from 7^2S to 5^2D. The relatively efficient $8^2S \to 6^2D$ ET may possibly be influenced by the $7^2P + 5^2S$ and $8^2P + 5^2S$ configurations. The ionic $Rb^+ + Rb^-$ term, which crosses the initial and final covalent states at large internuclear distances ($R > 60$ a.u.), may also contribute, although one would expect that this coupling is weak [14].

Our measured natural lifetimes (see Tab. 2) are in a very good agreement with those calculated by Theodosiou [21] and Hansen [22], and for the 6^2D state also with the theoretical lifetime of He *et al.* [23]. In order to compare them with the earlier experimental results [39–41], we should note that the lifetimes measured in [39,40] are not corrected for the BBR, no account for possible polarisation effects is reported in [39,41], and the fine structure of the 6^2D state was not distinguished in [41]. Thus the natural lifetimes given in [39,40] are slightly (by few ns) underestimated, since there is no BBR correction introduced This could explain why for the 8^2S state they are slightly lower than those of the present study and of [41].

The values for the 6^2D state of [39,41] may be affected by the fact that it was not ensured that relaxation of population and not of the alignment was registered. We cannot find, however, reasons for the 11% difference between the $6^2D_{3/2}$ lifetime measured in our study and the value given in [40]. Account for BBR in [40] would make it only larger.

In conclusion, we have measured the natural lifetimes and quenching cross-sections for $6^2D_{5/2,3/2}$ and $8^2S_{1/2}$ states, the 6^2D state J-mixing cross-section and the cross-section for ET from the 8^2S to 6^2D state. The analysis of time-resolved sensitised fluorescence signals allowed us to access information about the processes involved in the population transfer. The influence of the BBR on the population transfer can be significant even for such low lying states as 8^2S and 6^2D.

This work was partially supported by the Polish Committee for Scientific Research (grant No. 2 P03B 065 11) and by the Latvian Science Council. We gratefully acknowledge Prof. M. Auzins for helpful discussions and Prof. J. Migdałek for calculations of Rb oscillator strengths.

References

1. I.L. Beigman, V.S. Lebedev, Phys. Rep. **250**, 95 (1995).
2. P.H.T. Philipsen, J.H. Nijland, H. Rudolph, H.G.M. Heideman, J. Phys. B **26**, 939 (1993), and references therein.
3. Z.J. Jabbour, R.K. Namiotka, J. Huennekens, M. Allegrini, S. Milošević, F. de Tomasi, Phys. Rev. A **54**, 1372 (1996).
4. F. de Tomasi, S. Milošević, P. Verker, A. Fioretti, M. Allegrini, Z.J. Jabbour, J. Huennekens, J. Phys. B **30**, 4991 (1997).
5. V. Horvatic, C. Vadla, M. Movre, Z. Phys. D **27**, 123 (1993).
6. G. De Filippo, S. Guldberg-Kjær, S. Milošević, J.O.P. Pedersen, M. Allegrini, Phys. Rev. A **57**, 255 (1998).
7. V.M. Borodin, I.V. Komarov, Opt. Spektrosk. **36**, 250 (1974).
8. L. Barbier, M. Chéret, J. Phys. B **16**, 3213 (1983).
9. S. Geltman, Phys. Rev. A **40**, 2301 (1989).
10. P. Kowalczyk, J. Phys. B **17**, 817 (1984).
11. A.D. Sharma, H.A. Schuessler, R.H. Hill Jr, Phys. Rev. A **37**, 4649 (1988).
12. C. Gabbanini, L. Lucchesini, S. Gozzini, J. Phys. B **25**, 3145 (1992).
13. Luo Caiyan, A. Ekers, J. Klavins, M. Jansons, Phys. Scripta **53**, 306 (1996).
14. V. Grushevsky, M. Jansons, K. Orlovsky, Phys. Scripta **56**, 245 (1997); K. Orlovsky, V. Grushevsky, A. Ekers, Eur. Phys. J. D (submitted).
15. A. Ekers, Proc. Latv. Acad. Sci. B **7/8**, 130 (1995).
16. L. Barbier, M. Chéret, J. Phys. B **20**, 1229 (1987).
17. P. Hannaford, R.M. Lowe, Opt. Eng. **22**, 532 (1983).
18. W. Schade, L. Wolejko, V. Helbig, Phys. Rev. A **47**, 2099 (1993).
19. L. J. Curtis, P. Erman, J. Opt. Soc. Am. **67**, 1218 (1977).
20. T. F. Gallagher, in *Rydberg states of atoms and molecules*, edited by R.F. Stebbings, F. Barry Dunning (Cambridge University Press, 1982).
21. C.E. Theodosiou, Phys. Rev. A **30**, 2881 (1984).
22. W. Hansen, J. Phys. B **17**, 4833 (1984).
23. X. He, B. Li, A. Chen, C. Zhang, J. Phys. B **23**, 661 (1990).
24. M. Pimbert, J. Phys. **33**, 331 (1972).
25. A. N. Nesmeyanov, *Vapor pressure of the chemical elements* (Elsevier, Amsterdam/London/New York, 1963).
26. J. Migdałek, W.E. Baylis, Can. J. Phys. **57**, 1708 (1979).
27. J. Groszkowski, *Technika wysokiej prózni (High Vacuum Technique* - in Polish*)*, 2nd edn. (Wydawnictwa Naukowo-Techniczne, Warszawa, 1978); *Vacuum manual*, edited by L. Holland, W. Steckelmacher, J. Yarwood (E.&F.N. Spon, London, 1974).
28. J. Supronowicz, J.B. Atkinson, L. Krause, Phys. Rev. A **31**, 2691 (1985).
29. C.T. Ewing, D. Chang, J.P. Stone, J.R. Spann, R.R. Miller, J. Chem. Eng. Data **14**, 210 (1969).
30. R.E. Honig, RCA Rev. **23**, 567 (1967).
31. R. Hultgren, P.D. Desai, D.T. Hawkins, M. Gleiser, K.K. Kelley, D.D. Wagman, *Selected Values of the Thermodynamical Properties of the Elements* (American Society for Metals, Metals Park, Ohio, 1973).
32. J. Migdałek (private communication – the oscillator strengths calculated by using a fully relativistic model potential appeared to be quite close to the ones obtained with Coulomb approximation by A. Lindgård, S.E. Nielsen, At. Data Nucl. Data Tables **19**, 533 (1977).
33. B. Bieniak, A. Ekers, M. Głódź, J. Szonert (unpublished).
34. J. Szonert, B. Bieniak, M. Głódź, M. Piechota, Z. Phys. D **33**, 177 (1995).
35. V.S. Lebedev, Zh. Eksp. Teor. Fiz. [Sov. Phys. JETP] **103**, 50 (1993).
36. J.W. Parker, H.A. Schuessler, R.H. Hill Jr., B.G. Zollars, Phys. Rev. A **29**, 617 (1984).
37. J. Supronowicz, J.B. Atkinson, L. Krause, Phys. Rev. A **30**, 112 (1984).
38. M. Chéret, L. Barbier, Phys. Rev. A **30**, 1132 (1984).
39. J. Marek, P. Münster, J. Phys. B **13**, 1731 (1980).
40. H. Lundberg, S. Svanberg, Phys. Lett. A **56**, 31 (1976).
41. G. Waligórski, P. Kowalczyk, C. Radzewicz, Z. Phys. D **3**, 79 (1986).